Transfer Matrix Function (TMF) for Wave Propagation in Dielectric Waveguides With Arbitrary Transverse Profiles

Zion Menachem and Eli Jerby

***Abstract*—A transfer matrix function (TMF) is derived for the analysis of electromagnetic (EM) wave propagation in dielectric waveguides with arbitrary profiles, situated inside rectangular metal tubes. The TMF relates the wave profile at the waveguide output to the (arbitrary profile) input wave in the Laplace space. The TMF consists of the Fourier coefficients of the transverse dielectric profile and those of the input-wave profile. The method is applicable for inhomogeneous dielectric profiles with single or multiple maxima in the transverse plane. The TMF is useful for the analysis of dielectric waveguides in the microwave and the millimeter-wave regimes and for diffused optical waveguides in integrated optics.**

***Index Terms*—Dielectric waveguides, propagation.**

I. Introduction

DIELECTRIC waveguides and dielectric-loaded metallic waveguides have attracted a considerable interest in practice and theory [1]–[14] in a wide variety of transverse profiles. The purpose of this study is to develop transfer relations between the wave components at the output and input ports of such waveguides as matrix functions of their dielectric profiles. The approach presented in this paper is applicable for arbitrary profiles of the input field and of the dielectric, and is particularly useful for smoothly varying profiles.

Various methods for the analysis of similar problems (of wave propagation in dielectric inhomogeneous waveguides) have been studied in the literature. The review presented in [1] describes a wide range of homogeneous and inhomogeneous waveguides in the microwave and optical regimes. The main approaches discussed there are based on point matching, integral equations, finite differences, and finite elements. In [2], a variational formulation of the electromagnetic (EM) Maxwell equations is applied to dielectric-loaded rectangular waveguides. Reference [3] uses the method of finite differences to compute modes of dielectric guiding structures. The method of effective index is implemented in [4] in order to determine the dispersion of optical fibers with arbitrary cross-section shapes.

The modes of dielectric waveguides with arbitrary profiles are computed in [5] by a two-dimensional Fourier expansion. The scalar-wave equation is converted into a matrix eigenvalue equation by an expansion of the unknown field in a complete set of orthogonal functions. This expansion is applied to convert a linear partial differential equation into a matrix eigenvalue equation. Reference [6] presents modes of homogeneous and inhomogeneous lossless dielectric-slab rectangular waveguides. The Schrödinger equation is applied to dielectric waveguide problems in [7]. A domain-integral-equation method is proposed for the computational modeling of diffused channel waveguides [8]. This method is used in the design of channel waveguides realized by an ion-exchange process in glass substrates.

A general method to solve the scalar-wave equation for integrated optical devices is presented in [9]. The method is applied to three-dimensional problems with reflected waves by dividing the device into a series of sections of axially uniform waveguides. Guided modes of general dielectric waveguides are solved in [10] by expanding the unknown field vectors in sine series. Expansion of an arbitrary field in terms of waveguide modes using a Sturm–Liouville equation is presented in [11]. Scattering and transfer-matrix methods are used for modal analysis of lossy and amplifying waveguides [12], and for distributed-feedback devices [13], respectively. A review of the numerical and approximate methods for the modal analysis of general optical dielectric waveguides [14] discusses the methods of finite elements, finite differences, integral equations, series expansion, and separation of variables.

The following sections present the derivation of a transfer matrix function (TMF) for dielectric waveguides with arbitrary profiles. The method is applicable in general for lossy, as well as amplifying, dielectric media. It was first used to analyze waveguiding effects in free-electron lasers (FEL's), both in metal tubes and free space [15], [16]. In this paper, the TMF's are derived for passive lossless dielectric guides situated inside rectangular metallic tubes. The TMF computational algorithm is presented, and various examples are solved in order to demonstrate the TMF capabilities.

II. The TMF Derivation

A general scheme of a dielectric waveguide with an arbitrary profile in a rectangular metallic tube is shown in Fig. 1. The wave equations for the electric- and magnetic-field components in the inhomogeneous dielectric medium $\epsilon(x, y)$ are given by

$$\nabla^2\mathbf{E}+\omega^2\mu\epsilon\mathbf{E}+\bigtriangledown\left(\mathbf{E}\cdot\frac{\bigtriangledown\epsilon}{\epsilon}\right)=0 \qquad (1a)$$

Manuscript received June 25, 1996; revised December 22, 1997.

The authors are with the Department of Physical Electronics, Faculty of Engineering, Tel-Aviv University, Ramat Aviv 69978, Israel.

Publisher Item Identifier S 0018-9480(98)04952-7.

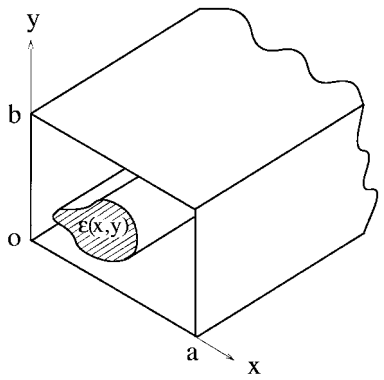

Fig. 1. A general scheme of an arbitrary profile dielectric waveguide.

and

$$\nabla^2\mathbf{H}+\omega^2\mu\epsilon\mathbf{H}+\frac{\nabla\epsilon}{\epsilon}\times(\nabla\times\mathbf{H})=0 \tag{1b}$$

respectively. The dielectric transverse profile is defined as

$$\epsilon(x,\,y)=\epsilon_0[1+\chi_0 g(x,\,y)] \tag{2}$$

where ϵ_0 represents the vacuum dielectric constant, χ_0 is the susceptibility of the dielectric material, and $g(x,\,y)$ is its profile function in the waveguide.

The normalized transverse derivatives of the dielectric profile $g(x,\,y)$ are defined as

$$g_x\equiv\frac{1}{\epsilon(x,\,y)}\left[\frac{\partial}{\partial x}\,\epsilon(x,\,y)\right] \tag{3a}$$

and

$$g_y\equiv\frac{1}{\epsilon(x,\,y)}\left[\frac{\partial}{\partial y}\,\epsilon(x,\,y)\right]. \tag{3b}$$

Using these definitions, the wave equation (1a) is written in the following form:

$$\nabla^2\mathbf{E}_x+k^2\mathbf{E}_x+\partial_x(\mathbf{E}_x g_x+\mathbf{E}_y g_y)=0 \tag{4a}$$
$$\nabla^2\mathbf{E}_y+k^2\mathbf{E}_y+\partial_y(\mathbf{E}_x g_x+\mathbf{E}_y g_y)=0 \tag{4b}$$
$$\nabla^2\mathbf{E}_z+k^2\mathbf{E}_z+\partial_z(\mathbf{E}_x g_x+\mathbf{E}_y g_y)=0 \tag{4c}$$

where k is the *local* wavenumber parameter, $k=\omega\sqrt{\mu\epsilon(x,\,y)}=k_0\sqrt{1+\chi_0 g(x,\,y)}$, and $k_0=\omega\sqrt{\mu_0\epsilon_0}$ is the free-space wavenumber.

The Laplace transform

$$\tilde{a}(s)=\mathcal{L}\{a(z)\}=\int_{z=0}^{\infty}a(z)e^{-sz}\,dz \tag{5}$$

is applied on the z-dimension, where $a(z)$ represents any z-dependent variables in (4a)–(4c). These are rewritten in the s-plane in the following form:

$$(\nabla_\perp^2+s^2+k^2)\tilde{E}_x+\partial_x(\tilde{E}_x g_x+\tilde{E}_y g_y)=sE_{x_0}+E'_{x_0} \tag{6a}$$
$$(\nabla_\perp^2+s^2+k^2)\tilde{E}_y+\partial_y(\tilde{E}_x g_x+\tilde{E}_y g_y)=sE_{y_0}+E'_{y_0} \tag{6b}$$
$$(\nabla_\perp^2+s^2+k^2)\tilde{E}_z+s(\tilde{E}_x g_x+\tilde{E}_y g_y)=sE_{z_0}+E'_{z_0}+(E_{x_0}g_x+E_{y_0}g_y). \tag{6c}$$

The transverse Laplacian operator is defined as $\nabla_\perp^2=\nabla^2-\partial^2/\partial z^2$, and E_{x_0}, E_{y_0}, E_{z_0} are the initial values of the corresponding fields at $z=0$, i.e., $E_{x_0}=E_x(x,\,y,\,z=0)$ and $E'_{x_0}=(\partial/\partial z)\,E_x(x,\,y,\,z)|_{z=0}$.

The use of the Laplace transform in the z-direction is preferred because it enables one to explicitly present the initial condition of the EM wave at the waveguide entrance. In addition, it displays (by the location of singularities on the complex s-plane) the convective instabilities of amplified or evanescent waves along media with inhomogeneous or complex dielectric constants.

A Fourier transform is applied on the transverse dimension

$$\overline{g}(k_x,\,k_y)=\mathcal{F}\{g(x,\,y)\}=\int_x\int_y g(x,\,y)\,e^{-jk_x x-jk_y y}\,dx\,dy \tag{7}$$

and the differential equation (6a)–(6c) are transformed to an algebraic form in the $(\omega,\,s,\,k_x,\,k_y)$ space as follows:

$$(s^2+k_z^2)\tilde{\overline{E}}_x+k_o^2\chi_o\overline{g}*\tilde{\overline{E}}_x+jk_x(\overline{g}_x*\tilde{\overline{E}}_x+\overline{g}_y*\tilde{\overline{E}}_y)=s\overline{E}_{x_0}+\overline{E}'_{x_0} \tag{8a}$$
$$(s^2+k_z^2)\tilde{\overline{E}}_y+k_o^2\chi_o\overline{g}*\tilde{\overline{E}}_y+jk_y(\overline{g}_x*\tilde{\overline{E}}_x+\overline{g}_y*\tilde{\overline{E}}_y)=s\overline{E}_{y_0}+\overline{E}'_{y_0} \tag{8b}$$
$$(s^2+k_z^2)\tilde{\overline{E}}_z+k_o^2\chi_o\overline{g}*\tilde{\overline{E}}_z+s(\overline{g}_x*\tilde{\overline{E}}_x+\overline{g}_y*\tilde{\overline{E}}_y)=s\overline{E}_{z_0}+\overline{E}'_{z_0}+(\overline{g}_x*\overline{E}_{x_0}+\overline{g}_y*\overline{E}_{y_0}) \tag{8c}$$

where $k_z=\sqrt{k_o^2-k_x^2-k_y^2}$. The asterisk symbol denotes the convolution operation

$$\overline{g}*\overline{E}=\mathcal{F}\{g(x,\,y)E(x,\,y)\}. \tag{9}$$

In order to solve the algebraic equations (8a)–(8c) numerically, the continuous $\mathbf{k}_\perp$ space is discretized to fundamental transverse wavenumbers $k_{ox}=\pi/a$ and $k_{oy}=\pi/b$, where a and b are the transverse dimensions of the rectangular boundaries. Hence, we substitute $k_x=nk_{ox}$ and $k_y=mk_{oy}$, where the integers n and m are truncated by $-N\le n\le N$ and $-M\le m\le M$, respectively. The orders N and M determine the accuracy of the solution, as shown in the convergence analysis in the following section.

In general, the TMF method is applicable for two kinds of waveguides: dielectric guides in free-space and dielectric-loaded metallic rectangular waveguides. In the first case, the (artificial) transverse boundaries a and b should be large enough to neglect the wave there. In the second case, the (real) metallic boundary conditions should be taken into account. This can be done by the method of images, as described below.

In order to solve the TMF for a dielectric-loaded metallic rectangular waveguide, the method of images is applied to satisfy the conditions $\hat{n}\times E=0$ and $\hat{n}\cdot(\nabla\times E)=0$ on the surface of the ideal metallic waveguide walls, where $\hat{n}$ is a unit vector perpendicular to the surface. The dielectric profile $g(x,\,y)$ is defined inside the waveguide boundaries $0\le x\le a$ and $0\le y\le b$. In order to maintain the boundary conditions without physical metallic walls, a substitute physical problem is constructed with infinite transverse extent. The periodicity

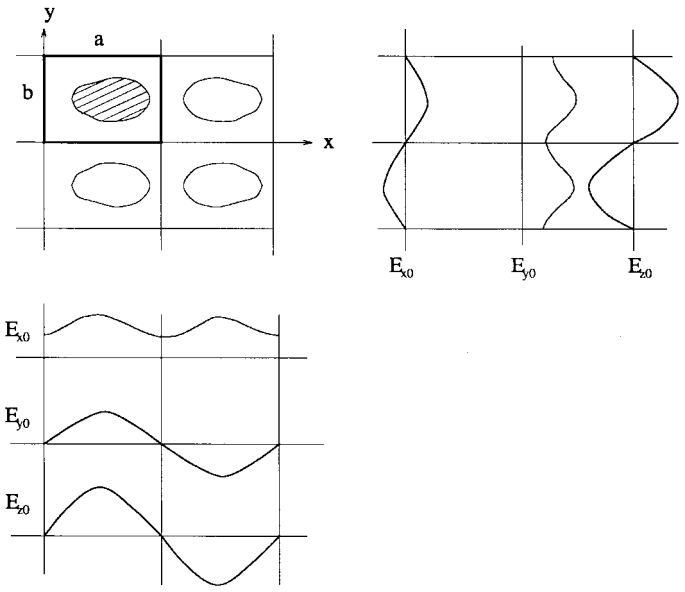

Fig. 2. The image method—substitution of metallic boundary condition by symmetrical and antisymmetric periodic continuation of images.

and the symmetry properties are chosen to force the boundary conditions at the location of the walls in the real problem. This is done by extending the waveguide region $0 \le x \le a$, $0 \le y \le b$ to a fourfold larger region, as shown in Fig. 2. Hence, the following relations are yielded:

$$g(-x, y) = g(x, -y) = g(x, y) = g(-x, -y) \tag{10a}$$

$$E_x(x, -y) = -E_x(x, y),\ E_x(-x, y) = E_x(x, y). \tag{10b}$$

The region $-a \le x \le a$, $-b \le y \le b$ is then further extended to infinity by periodic replication $g(x + 2\ell a, y + 2kb) = g(x, y)$, where $-\infty < \ell, k < \infty$. The field components, extended by an antisymmetric continuation in the $\hat{y}$-direction and by a symmetric continuation in the $\hat{x}$-direction, are periodically replicated in the same way, namely, $E_x(x + 2\ell a, y + 2kb) = E_x(x, y)$ for $-\infty < \ell, k < \infty$. The substitution of the physical problem is equivalent to the original problem in the region $0 \le x \le a$, $0 \le y \le b$ and satisfies the same boundary conditions on the boundary of this region. However, contrary to the original problem, it is infinite and periodic in the transverse dimensions. Therefore, it can be expanded by a discrete Fourier-transform series with $k_x = n\pi/a$ and $k_y = m\pi/b$. For dielectric waveguide in free space, or in cases where the metallic boundary conditions are negligible, the method of images is not needed and the computation of the TMF is simplified.

The Fourier components of the fields $\overline{E}(k_x, k_y)$ and of the other transverse functions in Fig. 8(a)–(c), with or without the image continuation, are discretized as

$$\overline{E}_{n,m} = \overline{E}(nk_{ox}, mk_{oy}) = \frac{1}{4ab}\int_{-a}^{a}\int_{-b}^{b} E(x, y)\cdot e^{-j(n(\pi/a)x + m(\pi/b)y)}\,dx\,dy \tag{11}$$

and form a spatial spectrum of plane waves. Its components are organized in a vectorial notation as follows:

$$\underline{\boldsymbol{E}} = \begin{bmatrix} \overline{E}_{-N,-M} \\ \vdots \\ \overline{E}_{-N,+M} \\ \vdots \\ \overline{E}_{+n,+m} \\ \vdots \\ \overline{E}_{+N,+M} \end{bmatrix}. \tag{12}$$

The convolution operation

$$\overline{g} * \overline{E} = \left\{ \sum_{n'=-N}^{N} \sum_{m'=-M}^{M} g_{n-n',m-m'}\, E_{n',m'} \right\} \tag{13}$$

is written in a matrix form as $\underline{\underline{\boldsymbol{G}}}\,\underline{\boldsymbol{E}}$ where $\underline{\underline{\boldsymbol{G}}}(n, m)(n', m') = g_{n-n',m-m'}$ and the matrix order is $(2N+1)(2M+1)$. The convolution operation is expressed by the cyclic matrix $\underline{\underline{\boldsymbol{G}}}$, which consists of Fourier components of the dielectric profile $\overline{g}_{nm}$, shown in (14), at the bottom of this page.

Equation (8a)–(8c) are rewritten in the following matrix form:

$$\underline{\underline{\boldsymbol{K}}}^{(0)}\underline{\boldsymbol{E}}_x + \frac{k_o^2\chi_0}{2s}\underline{\underline{\boldsymbol{G}}}\,\underline{\boldsymbol{E}}_x + \frac{jk_{ox}}{2s}\underline{\underline{\boldsymbol{N}}}\,(\underline{\underline{\boldsymbol{G}}}_x\,\underline{\boldsymbol{E}}_x + \underline{\underline{\boldsymbol{G}}}_y\,\underline{\boldsymbol{E}}_y) = \underline{\hat{\boldsymbol{E}}}_{x_0} \tag{15a}$$

$$\underline{\underline{\boldsymbol{K}}}^{(0)}\underline{\boldsymbol{E}}_y + \frac{k_o^2\chi_0}{2s}\underline{\underline{\boldsymbol{G}}}\,\underline{\boldsymbol{E}}_y + \frac{jk_{oy}}{2s}\underline{\underline{\boldsymbol{M}}}\,(\underline{\underline{\boldsymbol{G}}}_x\,\underline{\boldsymbol{E}}_x + \underline{\underline{\boldsymbol{G}}}_y\,\underline{\boldsymbol{E}}_y) = \underline{\hat{\boldsymbol{E}}}_{y_0} \tag{15b}$$

$$\underline{\underline{\boldsymbol{K}}}^{(0)}\underline{\boldsymbol{E}}_z + \frac{k_o^2\chi_0}{2s}\underline{\underline{\boldsymbol{G}}}\,\underline{\boldsymbol{E}}_z + \frac{1}{2}(\underline{\underline{\boldsymbol{G}}}_x\,\underline{\boldsymbol{E}}_x + \underline{\underline{\boldsymbol{G}}}_y\,\underline{\boldsymbol{E}}_y) = \underline{\hat{\boldsymbol{E}}}_{z_0} + \frac{1}{2s}(\underline{\underline{\boldsymbol{G}}}_x\,\underline{\boldsymbol{E}}_{x_0} + \underline{\underline{\boldsymbol{G}}}_y\,\underline{\boldsymbol{E}}_{y_0}) \tag{15c}$$

where the initial-value vectors $\underline{\hat{\boldsymbol{E}}}_{x_0}$, $\underline{\hat{\boldsymbol{E}}}_{y_0}$, and $\underline{\hat{\boldsymbol{E}}}_{z_0}$ consist of the transverse Fourier components of the input fields

$$\underline{\underline{\boldsymbol{G}}} = \begin{bmatrix} g_{00} & g_{-10} & g_{-20} & \cdots & g_{-nm} & \cdots & g_{-NM} \\ g_{10} & g_{00} & g_{-10} & \cdots & g_{-(n-1)m} & \cdots & g_{-(N-1)M} \\ g_{20} & g_{10} & \ddots & \ddots & \ddots & & \\ \vdots & g_{20} & \ddots & \ddots & \ddots & & \\ g_{nm} & \ddots & \ddots & \ddots & g_{00} & \vdots & \\ \vdots & & & & & & \\ g_{NM} & \cdots & \cdots & \cdots & \cdots & \cdots & g_{00} \end{bmatrix} \tag{14}$$

$(s\overline{E}_{x_0}+\overline{E}'_{x_0})/2s$, $(s\overline{E}_{y_0}+\overline{E}'_{y_0})/2s$, and $(s\overline{E}_{z_0}+\overline{E}'_{z_0})/2s$, and are organized in the form of (12). The field profile at the entrance to the waveguide can be substituted as any analytical function or numerical data according to the given problem.

The diagonal matrices $\underline{\underline{K}}^{(0)}$, $\underline{\underline{N}}$, and $\underline{\underline{M}}$ are defined as

$$\underline{\underline{K}}^{(0)}_{(n,m)(n',m')} = \{[k_o^2-(n\pi/a)^2-(m\pi/b)^2+s^2]/2s\} \cdot \delta_{nn'}\delta_{mm'} \tag{16a}$$

$$\underline{\underline{M}}_{(n,m)(n',m')} = m\delta_{nn'}\delta_{mm'} \tag{16b}$$

$$\underline{\underline{N}}_{(n,m)(n',m')} = n\delta_{nn'}\delta_{mm'} \tag{16c}$$

where $\delta_{nn'}$ and $\delta_{mm'}$ are the Kronecker delta functions.

The modified wavenumber matrices are defined as

$$\underline{\underline{D}}_x \equiv \underline{\underline{K}}^{(0)} + \frac{k_o^2\chi_0}{2s}\underline{\underline{G}} + \frac{jk_{ox}}{2s}\underline{\underline{N}}\,\underline{\underline{G}}_x \tag{17a}$$

$$\underline{\underline{D}}_y \equiv \underline{\underline{K}}^{(0)} + \frac{k_o^2\chi_0}{2s}\underline{\underline{G}} + \frac{jk_{oy}}{2s}\underline{\underline{M}}\,\underline{\underline{G}}_y \tag{17b}$$

$$\underline{\underline{D}}_z \equiv \underline{\underline{K}}^{(0)} + \frac{k_o^2\chi_0}{2s}\underline{\underline{G}} \tag{17c}$$

and (15a)–(15c) result in

$$\underline{\underline{D}}_x\underline{E}_x = \underline{\hat{E}}_{x_0} - \frac{jk_{ox}}{2s}\underline{\underline{N}}\,\underline{\underline{G}}_y\underline{E}_y \tag{18a}$$

$$\underline{\underline{D}}_y\underline{E}_y = \underline{\hat{E}}_{y_0} - \frac{jk_{oy}}{2s}\underline{\underline{M}}\,\underline{\underline{G}}_x\underline{E}_x \tag{18b}$$

$$\underline{\underline{D}}_z\underline{E}_z = \underline{\hat{E}}_{z_0} + 1/2s\,(\underline{\underline{G}}_x\underline{E}_{x_0} + \underline{\underline{G}}_y\underline{E}_{y_0}) - 1/2\,(\underline{\underline{G}}_x\underline{E}_x + \underline{\underline{G}}_y\underline{E}_y). \tag{18c}$$

After some algebraic steps, the TMF's are formulated as

$$\underline{E}_x = \left[\underline{\underline{D}}_x + \frac{k_{ox}k_{oy}}{4s^2}\underline{\underline{N}}\,\underline{\underline{G}}_y\underline{\underline{D}}_y^{-1}\underline{\underline{M}}\,\underline{\underline{G}}_x\right]^{-1} \cdot \left[\underline{\hat{E}}_{x_0} - \frac{jk_{ox}}{2s}\underline{\underline{N}}\,\underline{\underline{G}}_y\underline{\underline{D}}_y^{-1}\underline{\hat{E}}_{y_0}\right] \tag{19a}$$

$$\underline{E}_y = \left[\underline{\underline{D}}_y + \frac{k_{ox}k_{oy}}{4s^2}\underline{\underline{M}}\,\underline{\underline{G}}_x\underline{\underline{D}}_x^{-1}\underline{\underline{N}}\,\underline{\underline{G}}_y\right]^{-1} \cdot \left[\underline{\hat{E}}_{y_0} - \frac{jk_{oy}}{2s}\underline{\underline{M}}\,\underline{\underline{G}}_x\underline{\underline{D}}_x^{-1}\underline{\hat{E}}_{x_0}\right] \tag{19b}$$

$$\underline{E}_z = \underline{\underline{D}}_z^{-1}\Big[\underline{\hat{E}}_{z_0} + 1/2s\,(\underline{\underline{G}}_x\underline{E}_{x_0} + \underline{\underline{G}}_y\underline{E}_{y_0}) - 1/2\,(\underline{\underline{G}}_x\underline{E}_x + \underline{\underline{G}}_y\underline{E}_y)\Big]. \tag{19c}$$

The TMF's (19a)–(19c) describe the transfer relations between the spatial spectrum components of the output and input waves in the dielectric waveguide.

The transverse-field profiles are computed by the inverse Laplace and Fourier transforms as follows:

$$\underline{E}_y(x,y,z) = \sum_n\sum_m \int_{\sigma-j_\infty}^{\sigma+j_\infty} \underline{E}_y(n,m,s) \cdot e^{jnk_{ox}x+jmk_{oy}y+sz}\,ds. \tag{20a}$$

The inverse Laplace transform is performed in this study by a direct numerical integration on the s-plane by the method of Gaussian quadrature. The integration path in the right side

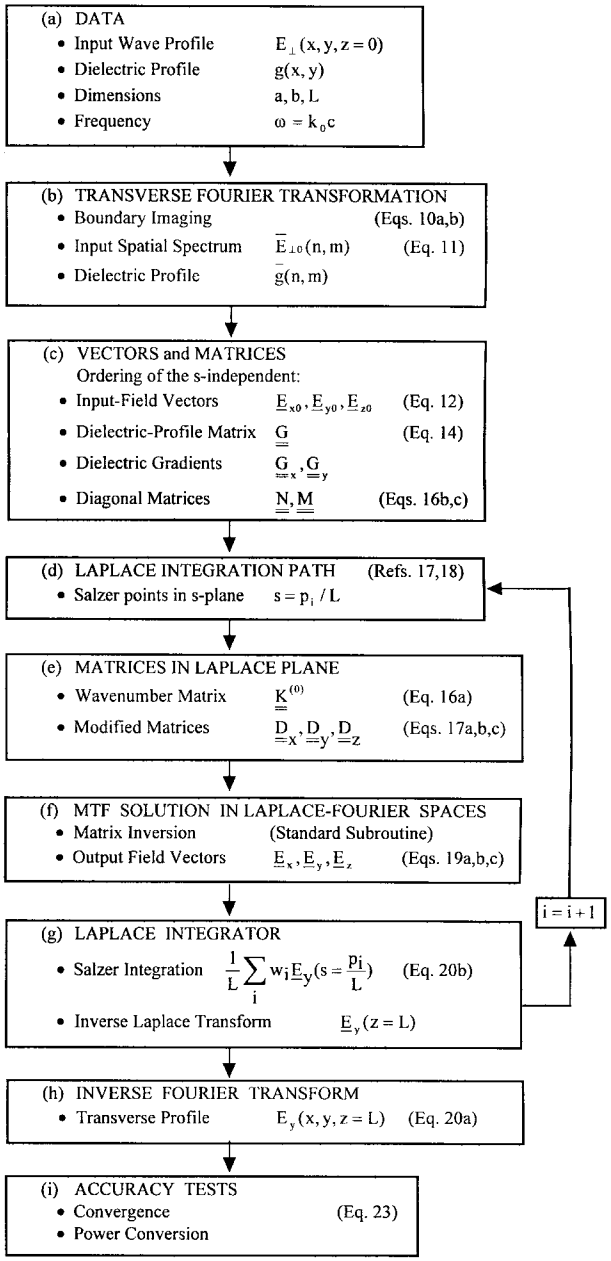

Fig. 3. A flowchart of the TMF computational algorithm.

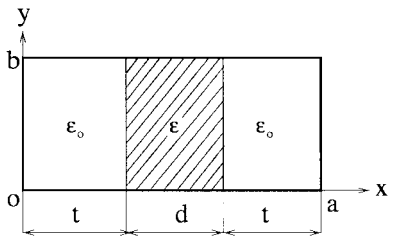

Fig. 4. A dielectric slab in a rectangular metallic waveguide.

of the s-plane includes all the singularities, as proposed by Salzer [17], [18] as follows:

$$\int_{\sigma-j_\infty}^{\sigma+j_\infty} e^{sL}\,\underline{E}_y(s)\,ds = \frac{1}{L}\int_{\sigma-j_\infty}^{\sigma+j_\infty} e^{p}\,\underline{E}_y(p/L)\,dp = \frac{1}{L}\sum_{i=1}^{15} w_i\underline{E}_y(s=p_i/L) \tag{20b}$$

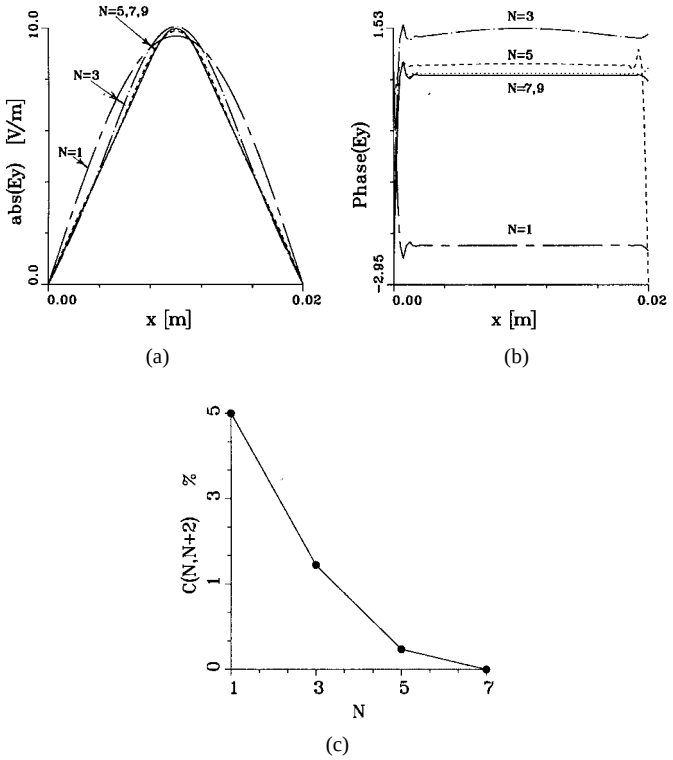

Fig. 5. A benchmark solution of the TMF (19) for a dielectric slab ($\epsilon_r = 9$, $a = 2$ cm, $b = 1$ cm, $d = 3.3$ mm, $L = 20$ cm, and $\lambda = 6.9$ cm) with the transcendental-equation mode (21a), (21b) as an input. (a) The wave amplitude solution of the TMF for $N = 1$–9. The solid line shows the transcendental-equation mode. (b) The output phase profile corresponding to Fig. 5(a). (c) The convergence of the TMF results.

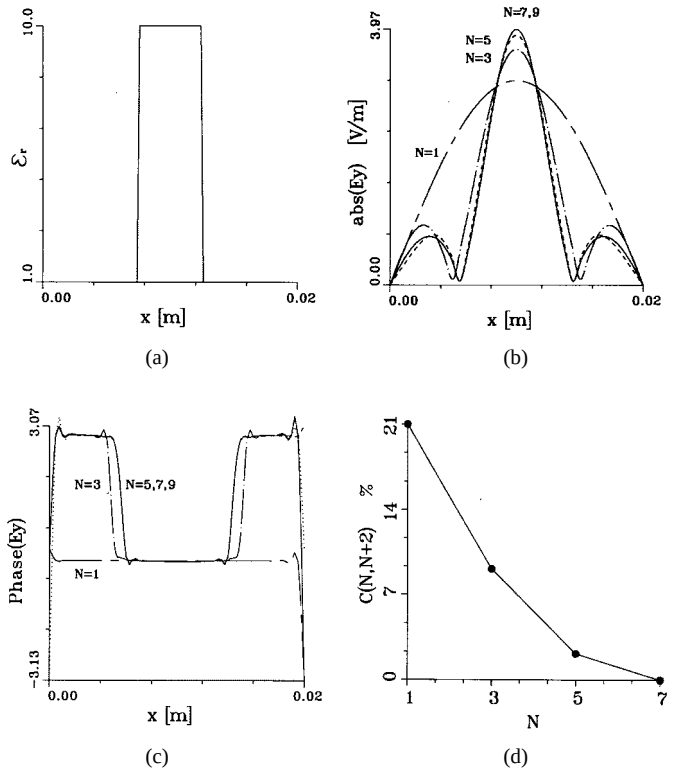

Fig. 6. A dielectric slab in a rectangular waveguide ($\epsilon_r = 10$, $a = 2$ cm, $b = 1$ cm, $d = 0.5$ cm, $L = 13$ and $\lambda = 3.75$ cm). (a) The slab profile. (b) The output field amplitude as response to a half-sine (TE_{10}) input-wave profile. (c) The output phase profile corresponding to Fig. 6(b). (d) The convergence of the TMF results (23).

where w_i and p_i are the weights and zeros, respectively, of the orthogonal polynomials of order 15 presented in [17] and [18]. The Laplace variable s is normalized by p_i/L in the integration points, where $\mathrm{Re}(p_i) > 0$ and all the poles should be localized in their left side on the s-plane. This approach of a direct integral transform does not require (as with other methods) dealing with each singularity separately. (An alternative approach could be to find the eigenmodes by the TMF eigenvectors and their wavenumbers by the associated eigenvalues. The input field could then be decomposed to those eigenmodes, propagated along the waveguide and composed again at the end. The direct inverse Laplace transform [17], [18] saves this effort by a robust solution of the TMF.)

A computational algorithm for the TMF solution is presented schematically by the flowchart shown in Fig. 3. Based on this recipe, a Fortran code was developed using NAG subroutines.[1] Several examples computed by this code [19] on a Unix system are presented in the following section.

III. Examples of TMF Applications

This section presents several examples which demonstrate features of the TMF derived in the previous section. First, the TMF model is applied to a dielectric slab with abrupt edges in a rectangular waveguide. The solution is compared to the results of the known transcendental equation as a benchmark. Second, the TMF is applied to solve problems of continuous dielectric profiles. In all the examples presented below, the wavelengths are in the centimeter range, the dimensions of the metallic rectangular tube are $a = 2$ cm and $b = 1$ cm, and the TMF orders are $N = M \leq 9$.

A. Dielectric Slab

The dielectric slab cross section in a rectangular metallic waveguide is shown in Fig. 4. Since its theoretical solution is known by other methods, this problem is used here as a benchmark for the TMF. Following [20], the solution for the wave propagation in a symmetrical slab is given by

$$E_{y1} = j\frac{k_z}{\epsilon_0}\sin(\nu x)\,e^{-jk_z z}, \qquad 0 < x < t \tag{21a}$$

$$E_{y2} = j\frac{k_z}{\epsilon_0}\frac{\sin(\nu t)}{\cos(\mu(t-a/2))}\cos[(\mu(x-a/2))]\,e^{-jk_z z}, \qquad t < x < a/2 \tag{21b}$$

where $\nu \equiv \sqrt{k_o^2 - k_z^2}$ and $\mu \equiv \sqrt{k_o^2\epsilon_r - k_z^2}$ result from the transcendental equation

$$\left(\frac{a}{d} - 1\right)\frac{\mu d}{2}\tan\left(\frac{\mu d}{2}\right) - (\nu t)\cot(\nu t) = 0 \tag{22}$$

for $\nu t \neq k\pi$ and $(\mu d/2) \neq (2k+1)(\pi/2)$. The solution obtained for the wave profile (21a), (21b) describes a symmetrical mode of the dielectric slab. For the benchmark, this

[1] The Numerical Algorithms Group (NAG) Ltd., Wilkinson House, Oxford, U.K.

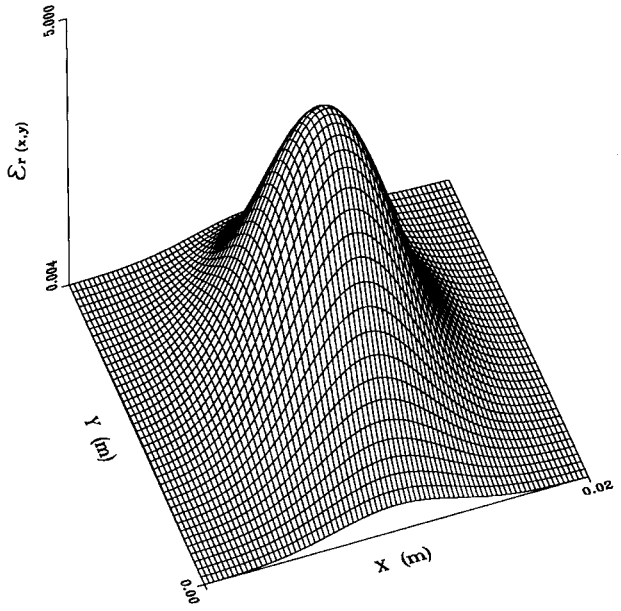

(a)

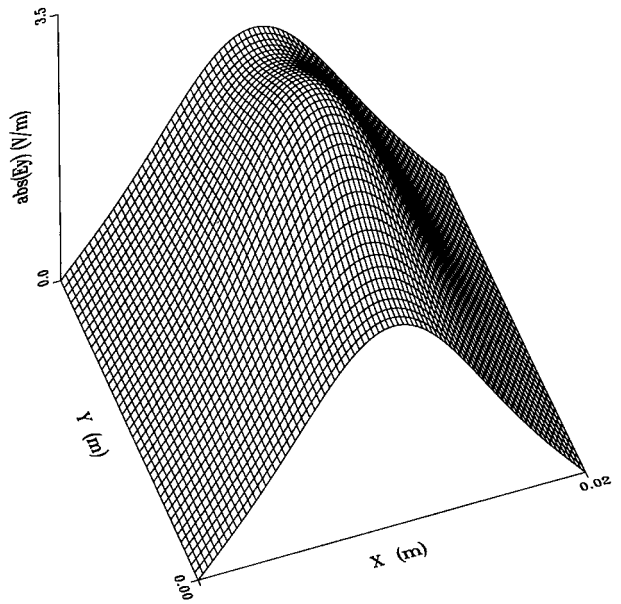

(b)

Fig. 7. A Gaussian dielectric waveguide ($a = 2$ cm, $b = 1$ cm, $L = 29$ cm, $\lambda = 3.75$ cm, and $N = 7$). (a) The Gaussian transverse profile of the dielectric waveguide $\epsilon_r(x, y)$. (b) The output wave profile in response to a half-sine (TE_{10}) input-wave profile.

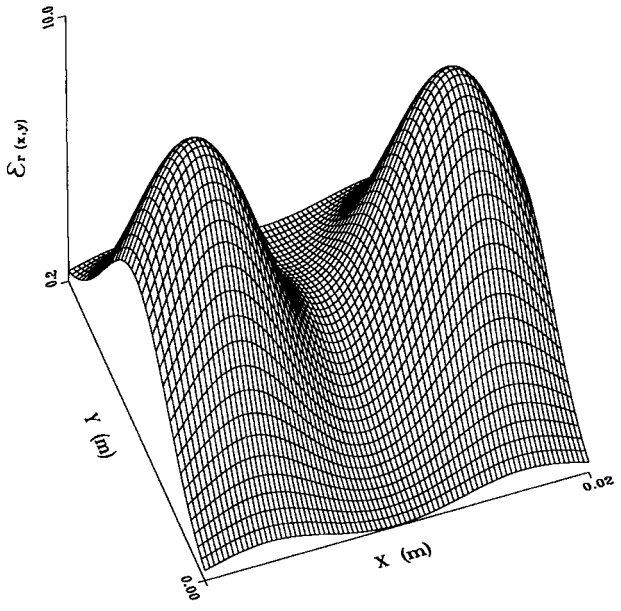

(a)

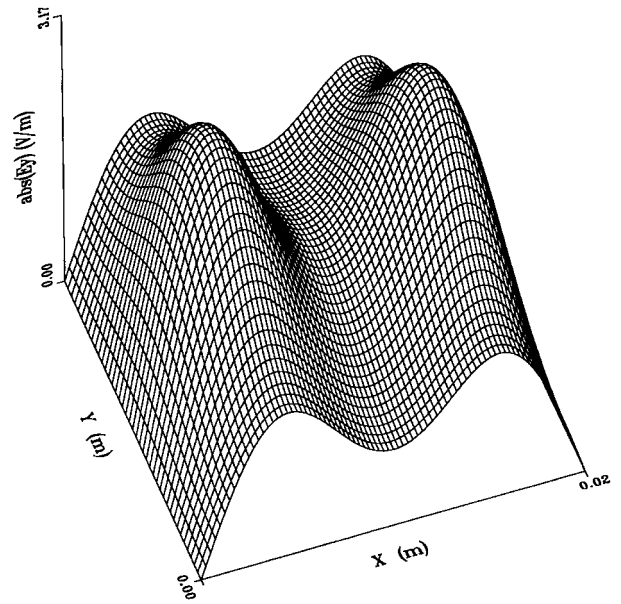

(b)

Fig. 8. Two dielectric waveguides with a double-humped Gaussian profile ($a = 2$ cm, $b = 1$ cm, $L = 18$ cm, $\lambda = 3.75$ cm, and $N = 7$). (a) The dielectric profile $\epsilon_r(x, y)$. (b) The output field profile as a response to a half-sine input-wave profile.

mode is substituted as an input wave at $z = 0$ to the TMF. The corresponding output resulting from the TMF is then compared to the original mode amplitude profile at $z = L$. The preservation along the waveguide (by the TMF) of the amplitude profile, which results from (21a) and (21b), provides a benchmark for the TMF accuracy, including the direct integration stage of the inverse Laplace transform.

Fig. 5(a) shows the resulting benchmark solution of the TMF for $N = 1$, 3, 5, 7, and 9, where the input is the fundamental mode (21a), (21b) and the other parameters are $\epsilon_r = 9$, $d = 3.3$ mm, and $\lambda = 6.9$ cm. The TMF results in Fig. 5(a) converge to the exact mode.

The corresponding phase profile is shown in Fig. 5(b). The convergence of the solution is verified by the criterion

$$C(N, N+2) \equiv \frac{\sum_x (|E_y(N+2) - E_y(N)|)}{\sum_x (|E_y(N+2)| + |E_y(N)|)}. \qquad (23)$$

The convergence rate of the peak amplitudes is shown in Fig. 5(c). An accuracy better than 1% is achieved in this example for $N \geq 5$, with respect to the exact solution of (21a) and (21b).

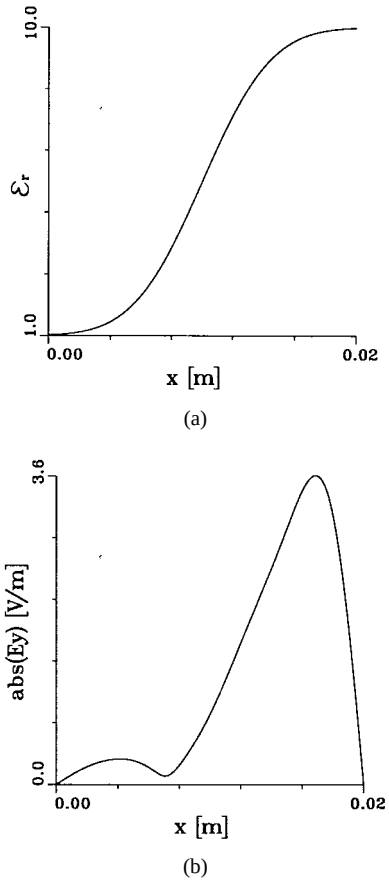

Fig. 9. A dielectric slab with a diffused edge ($\epsilon_r = 10$, $a = 2$ cm, $b = 1$ cm, $L = 33$ cm, $\lambda = 3.75$ cm, and $N = 9$). (a) The dielectric profile of a slab with a diffused edge profile. (b) The output field amplitude as a response to a half-sine input wave.

The response of the dielectric slab to an input-wave profile with a shape of a rectangular waveguide TE_{10} empty-waveguide mode is described in Fig. 6(a)–(c). The parameters of this example are $\epsilon_r = 10$, $d = 0.5$ cm, $L = 13$ cm, and $\lambda = 3.75$ cm. The dielectric profile is shown in Fig. 6(a). The resulting amplitude and phase profiles of the output wave are presented in Fig. 6(b) and (c), respectively, for $N = 1$–9. The convergence rate is shown in Fig. 6(d). For $N = 9$, the convergence rate in these conditions is $C = 0.1\%$.

B. Diffused Dielectric Waveguides

The ability of the TMF method to solve continuous problems is presented in this section by several examples of smoothly varying dielectric profiles. These examples include a Gaussian dielectric profile, a double-humped Gaussian profile, a dielectric slab with a diffused edge, and a composition of a Gaussian profile and a slab with a diffused edge. Continuous non-Gaussian profiles can be solved as well by the TMF method.

The first example shown in Fig. 7(a) is a Gaussian dielectric profile in the form

$$\epsilon_r(x, y) = 5 \exp\left[\frac{-(x - a/2)^2}{p_x^2}\right] \exp\left[\frac{-(y - b/2)^2}{p_y^2}\right]. \tag{24}$$

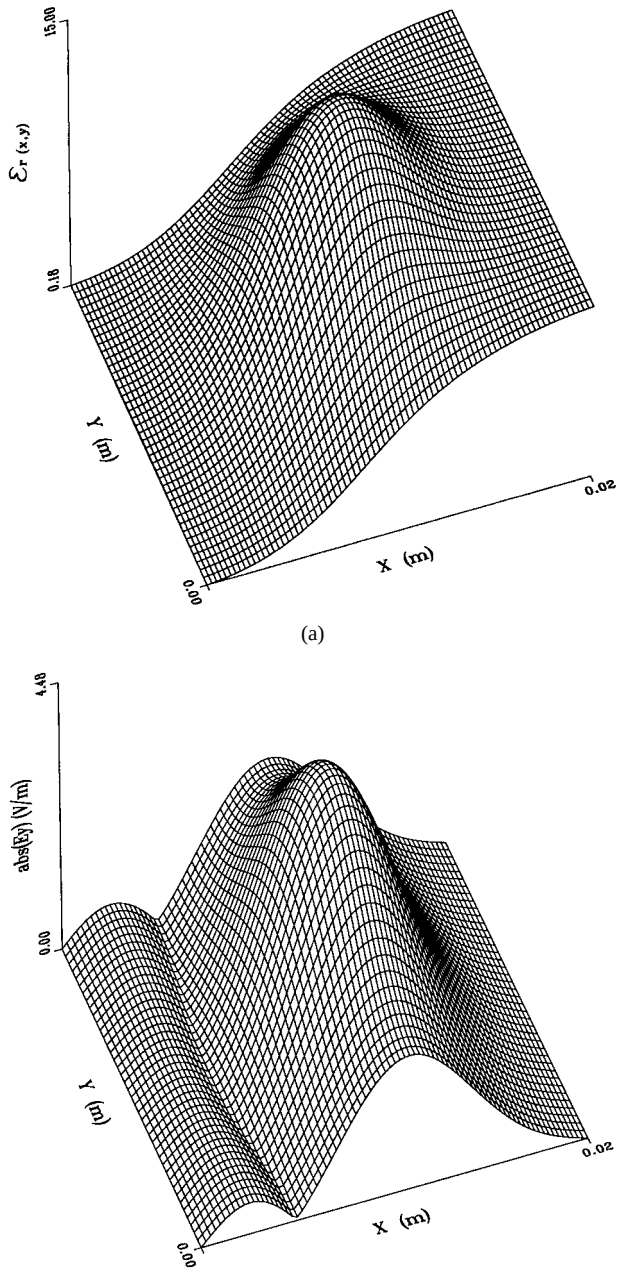

Fig. 10. A composition of a Gaussian profile dielectric rod and a slab with a diffused edge ($a = 2$ cm, $b = 1$ cm, $L = 17$ cm $\lambda = 3.75$ cm, and $N = 9$). (a) The dielectric profile $\epsilon_r(x, y)$. (b) The output filed profile as a response to a half-sine input wave profile.

Equation (3a) and (3b) result in $g_x(x, y) = -[2(x - a/2)]/p_x^2$ and $g_y(x, y) = -[2(y - b/2)]/p_y^2$. The input waves are chosen arbitrarily as the profile of the TE_{10} of the empty waveguide. Fig. 7(b) shows the wave profile evolved in this waveguide as the result of this input-wave profile, for $p_x = 7$ mm, $p_y = 5$ mm, and $\lambda = 3.75$ cm. Both the half-sine (TE_{10}) profile and the Gaussian shape emerge in the output wave profile.

A dielectric profile with double-humped Gaussian shape is shown in Fig. 8(a). The centers of the two Gaussian slabs are located at $x_1 = a/6$, $y_1 = b/2$, and $x_2 = 5a/6$, $y_2 = b/2$. The wave profile evolved as a result of an (arbitrary) input

as a TE_{10} mode is shown in Fig. 8(b). The result shows that the radiation power is split between the two diffused dielectric waveguides.

A diffused-slab waveguide profile is shown in Fig. 9(a). The output wave profile for the same parameters, as in the previous example, is seen in Fig. 9(b). In another example, a Gaussian channel is diffused on top of the slab continuous edge, as shown in Fig. 10(a). The output wave profile is presented in Fig. 10(b). The waveguiding is clearly observed in the resulting duct effect.

IV. Discussion

The TMF approach presented in this paper provides a numerical tool for the calculation of wave propagation in arbitrary shaped dielectric waveguides. The model is applicable for continuous transverse dielectric profiles and for arbitrary input-wave distributions. The evolution of the wave along the waveguide is computed by *input–output* matrix relations (19a)–(19c).

The numerical solutions presented in this paper show a variety of examples of the TMF features. The model can be used to find eigenmodes of the dielectric waveguide and to analyze coupling between adjacent dielectric waveguides.

The TMF model is especially applicable to continuous problems (i.e., smoothly varying profiles) in which the dimensions of the transverse variations are of the order of the EM wavelength. In these cases, the TMF provides reasonable accuracy and computation time.

The TMF might be a useful tool for the analysis of continuous dielectric waveguides in the microwave and millimeter-wave regimes and for diffused waveguides in integrated optics [21]. Applications of the TMF to lossy and amplifying dielectric media in metal boundaries and in free space will be presented in the future.

References

[1] S. M. Saad, "Review of numerical methods for the analysis of arbitrarily shaped microwave and optical dielectric waveguides," *IEEE Trans. Microwave Theory Tech.*, vol. MTT-33, pp. 894–899, Oct. 1985.

[2] W. J. English, "A computer-implemented vector variational solution of loaded rectangular waveguides," *SIAM J. Appl. Math.*, vol. 21, pp. 461–468, 1971.

[3] E. Schweig and W. Bridges, "Computer analysis of dielectric waveguides: A finite-difference method," *IEEE Trans. Microwave Theory Tech.*, vol. MTT-32, pp. 531–541, May 1984.

[4] K. S. Chiang, "Analysis of optical fibers by the effective-index method," *Appl. Opt.*, vol. 25, pp. 348–354, 1986.

[5] C. H. Henry and B. H. Verbeek, "Solution of the scalar wave equation for arbitrarily shaped dielectric waveguides by two-dimensional Fourier analysis," *J. Lightwave Technol.*, vol. 7, pp. 308–313, Feb. 1989.

[6] Y. Cheng-Cheh and C. Tah-Hsiung, "Analysis of dielectric-loaded waveguide," *IEEE Trans. Microwave Theory Tech.*, vol. 38, pp. 1333–1337, Sept. 1990.

[7] M. Munowitz and D. J. Vezzetti, "Application of the Fourier-grid method to guided-wave problems," *J. Lightwave Technol.*, vol. 8, pp. 889–893, June 1990.

[8] N. H. C. Baker, M. B. J. Diemeer, J. M. van Splunter, and H. Blok, "Computational modeling of diffused channel waveguides using a domain integral equation," *J. Lightwave Technol.*, vol. 8, pp. 576–586, Apr. 1990.

[9] C. H. Henry and Y. Shani, "Analysis of mode propagation in optical waveguide devices by Fourier expansion," *IEEE J. Quantum Electron.*, vol. 27, pp. 523–530, Mar. 1991.

[10] D. Marcuse, "Solution of the vector wave equation for general dielectric waveguides by the Galerkin method," *IEEE J. Quantum Electron.*, vol. 28, pp. 459–465, Feb. 1992.

[11] A. Hardy and M. Ben-Artzi, "Expansion of an arbitrary field in terms of waveguide modes," *Proc. Inst. Elect. Eng., Optoelectron.*, vol. 141, pp. 16–20, 1994.

[12] T. D. Visser, H. Blok and D. Lenstra, "Modal analysis of a planar waveguide with gain and losses," *IEEE J. Quantum Electron.*, vol. 31, pp. 1803–1810, Oct. 1995.

[13] J. Hong, W. P. Huang, and T. Makino, "On the transfer matrix method for distributed-feedback waveguide devices," *J. Lightwave Technol.*, vol. 10, pp. 1860–1868, Dec. 1992.

[14] K. S. Chiang, "Review of numerical and approximate methods for the modal analysis of general optical dielectric waveguides," *IEEE J. Quantum Electron.*, vol. 26, pp. S113–S134, June 1994.

[15] E. Jerby and A. Gover, "Wave profile modification in Raman free-electron lasers: Space-charge transverse fields and optical guiding," *Phys. Rev. Lett.*, vol. 63, pp. 864–867, 1989.

[16] ———, "A linear 3D model for free-electron lasers," *Nucl. Instrum. Methods Phys. Res. A, Accel. Spectrom. Detect. Assoc. Equip.*, vol. A285, pp. 864–867, 1989.

[17] H. E. Salzer, "Orthogonal polynomials arising in the numerical evaluation of inverse Laplace transforms," *Math. Tables Other Aids to Comput*, vol. 9, pp. 164–177, 1955.

[18] ———, "Additional formulas and tables for orthogonal polynomials originating from inversion integrals," *J. Math. Phys.*, vol. 39, pp. 72–86, 1961.

[19] Z. Menachem, "Matrix transfer function (MTF) for wave propagation in dielectric waveguides with arbitrary transverse profiles," M.Sc. thesis, Faculty of Eng., Tel-Aviv Univ., Ramat Aviv, Israel, 1996.

[20] R. E. Collin, *Foundation for Microwave Engineering.* New York: McGraw-Hill, 1966.

[21] T. Tamir, *Guided-Wave Optoelectronics.* Berlin, Germany: Springer-Verlag, 1988.

Zion Menachem received the M.Sc. degree from Tel-Aviv University, Ramat Aviv, in 1996, and is currently working toward the Ph.D. degree investigating wave propagation in curved waveguides.

Eli Jerbywas born in Israel, in 1957. He received the M.Sc. and Ph.D. degrees in electrical engineering from Tel-Aviv University (TAU), Ramat Aviv, in 1980 and 1989 respectively.

From 1989 to 1990, he was a Rothschild and Fulbright Post-Doctoral Fellow in the Research Laboratory of Electronics, Massachusetts Institute of Technology (MIT), Cambridge, and a Visiting Scientist in the summers of 1991 and 1992. Upon his return to TAU, he established the High-Power Microwave Laboratory, where along with his graduate students and research fellows, he studies novel schemes of microwave radiation sources and their practical applications. Since 1994, he has been a tenured Senior Lecturer at TAU, where he teaches and develops courses on microwave engineering. His projects for industry are contracted through Ramot Ltd. He has served on the Program Committees of International FEL Conferences in the U.S., Europe, and Japan. He served as chair of the International Research Workshop on Cyclotron-Resonance Masers and Gyrotrons of the Israeli Academy of Sciences and Humanities (Israel, May 1998).

Dr. Jerby served as a co-guest-editor of a special issue on cyclotron-resonance masers and gyrotrons of the IEEE Transactions on Plasma Science.